ACS OMEGA

Open Access

This article is licensed under CC-BY-NC-ND 4.0

http://pubs.acs.org/journal/acsodf

Article

Bioengineered Smart Nanocarriers for Breast Cancer Treatment: Adorned Carbon-Based Nanocomposites with Silver and Palladium Complexes for Efficient Drug Delivery

Moein Safarkhani, Sadaf Saboori Moghaddam, Fahimeh Taghavimandi, Mojtaba Bagherzadeh,* Yousef Fatahi, Uichang Park, Fatemeh Radmanesh, Yun Suk Huh,* and Navid Rabiee

Cite This: *ACS Omega* 2024, 9, 1183−1195

Read Online

ACCESS | Metrics & More | Article Recommendations | Supporting Information

ABSTRACT: Biocompatible and bioactive carbon-based nanocomposites are ingeniously designed and fabricated with the aim of enhancing drug delivery applicability in breast cancer treatment. Reduced graphene oxide (rGO) and multiwalled carbon nanotubes (MWCNTs) are utilized as nanocarriers for increasing penetrability into cells and the loading capacity. What sets our study apart is the strategic incorporation of the two different complexes of silver (AgL_2) and palladium (PdL_2) with the carboxamide-based ligand $C_9H_7N_3OS$ (L), which have been synthesized and decorated on nanocarriers alongside doxorubicin (DOX) for stabilizing DOX by $\pi-\pi$ interactions and hydrogen bonding. Although DOX is a well-known cancer therapy agent, the efficacy of DOX is hindered owing to drug resistance, poor internalization, and limited site specificity. Aside from stabilizing DOX on nanocarriers, our carbon-based nanocarriers are tailored to act as a precision-guided missile, strategically by adorning with target-sensitive complexes. Based on the literature, carboxamide ligands can connect to overexpressed receptors on cancerous cells and inhibit them from proliferation signaling. Also, the complexes have an antibacterial activity that can control the infection caused by decreasing white blood cells and necrosis of cancerous cells. A high-concentration cytotoxicity assay revealed that decorating PdL_2 on a DOX-containing nanocarrier not only increased cytotoxicity to breast cancerous cell lines (MDA-MB-231 and MCF-7) but also revealed higher cell viability on a normal cell line (MCF-10A). The drug release screening results showed that the presence of PdL_2 led to 72 h correlate release behavior in acidic and physiological pH profiles, while the AgL_2 containing nanocomposite showed an analogue behavior for just 6 h and the release of DOX continued and after about 100 h hit the top.

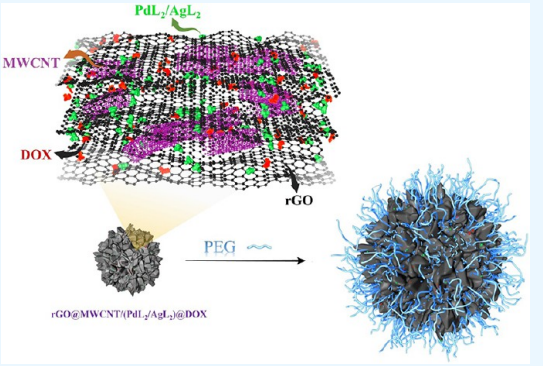

1. INTRODUCTION

The expected life cycle of cells is growth and multiplication, creating new cells. Changes in DNA within cells cause uncontrollable growth that leads to cancer.[1] Cancer is one of the most common causes of death all around the world (~40,000 die just in the United States, annually). There are numerous differences between healthy and cancerous cell growth, and ignoring of stop signals, appearance, and size of the nucleus are some of them. Some cancer cells can freely spread into other tissues because of defects in unnatural growth, a function called metastasis. The path of spread is through lymphatic or blood vessels.[2,3] There are various treatments for cancer, such as surgery, immunotherapy,[4] chemotherapy,[5] hormone therapy,[6] and radiotherapy,[7] but it is a high priority to examine the primary tumor before choosing the proper treatment.[8] There are over 200 different types of cancer cells that are varied in size, shape, and lifetime. One of the most common and widespread cancers is breast cancer. Various parts of the breast can be cancerous, which leads to different breast tumors as follows: (a) phyllodes tumor (develops in the breast stroma, mostly benign, rare), (b) invasive ductal or lobular carcinoma (IDC: starts from the breast milk duct and develops to breast fatty tissue, the most frequent breast cancer type; ILC: starts from the breast milk glands, the second most common, about 15% of all breast cancers), (c) ductal carcinoma *in situ* (noninvasive, develops and stays only in the breast milk duct lining), (d) breast Paget disease (starts from milk ducts and develops to the areola and nipple skin, rare), (e) angiosarcoma (starts from lymph or line blood vessels, spreadable to tissue or breast skin), (f) triple-negative breast cancer (lack of progesterone, estrogen, and HER2, very aggressive and laborious treatment), and (g) positive or negative HER2 (the

Received: September 26, 2023
Revised: November 28, 2023
Accepted: November 29, 2023
Published: December 18, 2023

© 2023 The Authors. Published by American Chemical Society

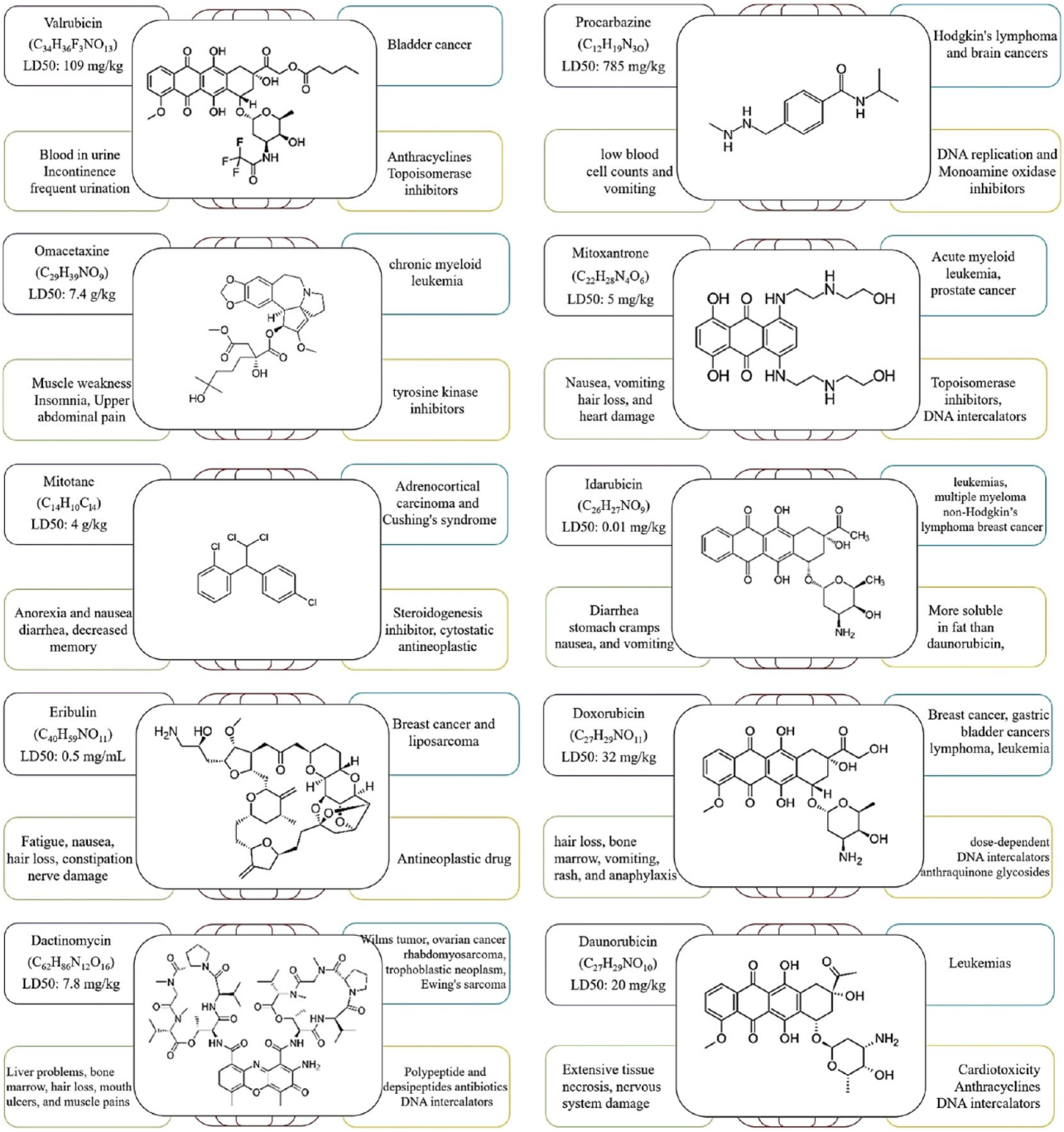

Figure 1. Most frequent medicines and their biochemical features. Black box: chemical structure; purple box: identifications; blue box: cancer types; green box: side effects; yellow box: features.

positive type has a tendency to grow fast, and the negative type does not show any response to HER2-targeting drugs). Although it is not common, men also may suffer from breast cancer and the most reported types are ILC and IDC. Every type of these breast tumors needs special prognosis and treatment, which vastly depend on cancer stage, grade, expression of receptors, age and sex of the patient, and overall health.[9−11]

Chemotherapy treats undetectable free cancer cells by using chemicals to stop or slow their multiplication and growth. However, this function can slow down other fast-growing healthy cells like hair and cause other side effects like fatigue, nausea, vomiting, and death in some extreme cases.[12] Researchers are looking for chemicals with higher effectiveness and fewer side effects.[13] Another obstacle to chemotherapy is multidrug resistance (MDR), which enables tumorous cells to escape by increasing resistance to drugs. The tumorous cells' instinct leads to drug resistance by overgrowing some receptor-like proteins on the mutated cells' surface, and this approach tries to restrict cell membrane access with a conventional drug. For instance, mutated cells decrease the P-glycoprotein that is responsible for the transfer of doxorubicin (DOX) inside the cell and increase B-cell lymphoma 2, which is an antiapoptosis protein. These chemotherapy limits have led to the evolution of smart drug delivery systems (SDDSs).[14] The reduction of cancer treatment's limitations has occurred thanks to the emergence of nanocarriers.

https://doi.org/10.1021/acsomega.3c07432
ACS Omega 2024, 9, 1183−1195

Due to the presence of difficulties, chemical delivery is limitedly used in chemotherapy (local or metastatic tumors). The major ordeal would be the cancerous cells' accessibility limitation.[15] Researchers are constantly searching for ways to address problems such as lowering the injection frequency, using lower doses of chemicals, and eliminating chemotherapeutics' side effects for cancer patients during chemotherapy.[16] A small molecule's delivery is very much dependent on the tumor's physicochemical properties. The first focus of improving drug delivery was solubility, increasing selectivity, and controlling drug release.[17] Low selectivity in delivery and uncontrollable drug release in rudimentary drug delivery systems led to the development of SDDSs.[14] In the past few years, SDDSs have attracted the most inquiries as chemical deliverers to overcome predicaments, such as low chemotherapeutic loading capacity, bleeding of the drugs before reaching the targeted cells, and limitation of cell penetration owing to aggregation of new drugs.[18] Nanocarriers can benefit the treatment process by releasing drugs in the tumor microenvironment (TME).

Savjani et al. reported that chemotherapeutic drugs mostly have poor solubility in water and the most important requisite for absorbing a drug is it being in the form of a solution.[19,20] The DOX water solubility is about 50 mg/mL. Nanocarriers with unique properties fix issues such as solubility, good drug release profile, hydrophilicity, size, high specificity, and enhanced permeability and retention effect.[8] Among all nanocarriers, carbon-based ones have the most frequent usage in the delivery field due to their distinctive features like binding to the cell membrane, which prepares the best place for DOX release, and also this binding can induce cell membrane ruffling that can stimulate cell stress, which leads to apoptosis, methuosis, and generation of ROS.[21] Based on Mirza-Aghayan et al.'s study, nanocarriers can enter tumorous cells through endocytosis.[22] Graphene oxide (GO) has hydroxyl (−OH), carbonyl (C═O), alkoxy (C−O−C), carboxylic acid (−COOH), and other functional groups with oxygen based on the literature, will all lead to increasing the cytotoxicity.[16,23] Reduced graphene oxide (rGO) can easily be obtained from GO by thermal, chemical, or UV light reduction that leads to a decrease in the number of O-containing functional groups. A carbon nanotube (CNT) is another carbon allotrope in the shape of an empty cylinder, and it is produced by rolling up a graphene sheet.[24,25] SWCNTs have a diameter of about a nanometer.[26,27] For preparing more space between rGO layers, multiwalled carbon nanotubes (MWCNTs) have been utilized among rGO sheets to study their prospective effects on loading efficiency.[28] Overall, the MWCNT and rGO loading capacity was limited, and in the present project, we aim to study their synergetic effect on the loading and release of a drug.

The main concern about delivering the cargo onto the goal site is finding an efficient way to manage the drug loading and release process.[29] One last novel approach for inhibition of drug bleeding was utilizing the drugs as a ligand of transition metal complexes; Marloye et al. in the past decade conducted a survey and studied this kind of delivery system. Although the mentioned method was promising drug release to hinder the release before targeted sites, it decreased drug efficiency due to occupying the drug's effective functional groups by metal.[30] It is noticeable that most anticancer drugs after connecting to the specific on-cell receptors can control the cells' proliferation or metastasis path.[31] On the other side of the coin, some in-lab-prepared ligands can act as an inhibitor of special on-cell receptors.[32] Their bioactive functional groups after coordination with the metal are free or can be freed. Theoretically, complexes that coordinate with the ligands can assist the drug to attach better to the nanocarrier's surface with their aromatic rings ($\pi-\pi$ interaction). The medicines usually used in chemotherapy, especially DOX, have benzene. The $\pi-\pi$ interactions help the drug connect more firmly to the nanocarrier's surface, and this operation prevents premature bleaching (bleeding). Different metals have different levels of toxicity to the human body, so their applicability is much limited. The acceptable ones are the ones that can mimic Pt and Fe in-the-body interactions. After reviewing recently published papers on biocompatible metals,[33] Ag and Pd are found to be more suitable than the others due to their distinctive features like biocompatibility and cost-effectiveness. In this article, the behaviors of Ag and Pd complexes in drug loading and release efficiency are compared. The usual functional groups of ligands of synthesized complexes in biomaterial or bioapplications are carbonyl, amino, methyl, hydroxyl, and sulfhydryl.[34] Carboxamides are a desirable functional group among all, thanks to having both carbonyl and amino functional groups beside each other, which leads to unique features.[35] Based on biomedical studies, carboxamides are so promising because they can connect to overexpressed on-the-cell receptors and disrupt their uncontrolled functionality and also have DNA intercalation ability, which is a trigger of apoptosis.[36,37] Cancer treatments have shifted from one drug for all types (for instance, DOX has been widely used for the treatment of breast, stomach, lung, testicle, and ovary cancers[38]) to a more specific treatment for each patient in the past few years. Biochemical and biomedical scientists' findings give physicians more options to remedy each type of cancer by taking a more relatable and effective drug.[39] A summary of typical cancer drugs and their effectiveness is provided in Figure 1.

The most essential part of preparing site-specific nanocarriers is the coating, which does not let the whole structure become fragmented before arriving at the TME. Additionally, based on the literature, coated nanocarriers have been revealed to have considerably lower cytotoxicity compared with noncoated ones (unattacked by microphages) and the final size of the prepared nanocarriers could be smaller after utilizing coating agents (the smaller the structures, the better the cell penetration and clearness after drug release). The published papers in the biological field have disclosed that overexpressed MUC1 on-the-cell receptors have a potent tendency to connect to glycans.[40] Poly(ethylene glycol) (PEG) has been considerably utilized for functionalizing various nanocarriers to more efficiently deliver drugs/genes for cancer treatment and is a water-soluble polymer used as a nonionic polymer in drug delivery.[41] Nanocarriers should circulate in the blood system as much as possible to convey sufficient concentrations of the systematic treatment content (drugs and other therapeutic agents) to targeted tissues. PEGylation can decrease the immunogenicity of proteins and increase the systematic circulation time.[42,43] The cells' glutathione can dissociate PEG from nanocarriers.[21] The different conformations of PEG are brush and mushroom conformations, depending on the surface graft density. The degree of PEG layer thickness depends upon the conformation, molecular weight, and reaction time. In the case of PEGs, the molecular weight mainly controls the half-life of PEG.[44]

Based on all of the abovementioned information and published surveys in this field, defects and needs led us to design an efficient carbon-based nanocomposite decorated with complexes of Ag or Pd and coated with PEG for delivering DOX site-specifically and efficiently to cancerous cells.

https://doi.org/10.1021/acsomega.3c07432
ACS Omega 2024, 9, 1183−1195

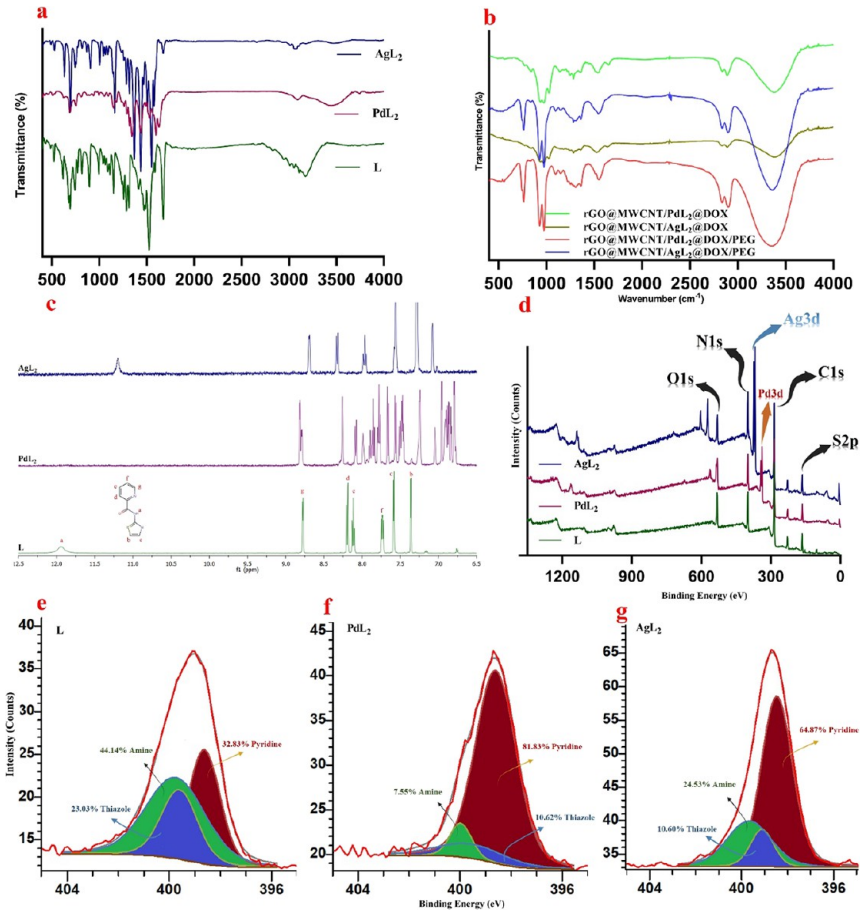

Figure 2. FT-IR spectra of (a) L, PdL_2, and AgL_2 and (b) fabricated nanocomposites; (c) ^1H NMR spectra of L, PdL_2, and AgL_2; (d) XPS survey of L, PdL_2, and AgL_2; (e) N 1s survey of L; (f) N 1s survey of PdL_2; (g) N 1s survey of AgL_2.

2. MATERIALS AND METHODS

Solvents and all chemicals were commercial reagent grade purchased from Fluka and Merck and utilized as soon as possible after receiving them without any further purifications. A Unicam Maston 1000 FT-IR spectrophotometer (400−4000 cm^{-1} in KBr pellets and at room temperature) was utilized for recording the FT-IR spectra. A Bruker FT-NMR 500 MHz spectrometer (the chemical shift of protons is reported in parts per million (ppm) in $CDCl_3$ and DMSO-d_6) was used for obtaining the ^1H NMR spectra of L, AgL_2, and PdL_2. A Cary 100 Bio Varian spectrophotometer (10 mm path length, quartz cell) was used for UV−Vis analysis. The carboxamide-based ligand was synthesized and was characterized by different methods. The palladium metal ion solution was obtained from its acetate salt, and the silver metal ion was synthesized from its chloride salt.

2.1. Synthesis of Ligand L (*N*-(Thiazol-2-yl)-picolinamide). For the synthesis of $C_9H_7N_3OS$ (*N*-(thiazol-2-yl)picolinamide; MW: 205.24), instead of utilizing the nongreen synthesis method that has been reported by Juhas et al.,[45] we chose the ionic liquid method, which is greener and more environmentally friendly. So, precise amounts of TBAB (10 mmol, 3.22 g), triphenylphosphite (20 mmol, 6.44 g), 2-aminothiazole (20 mmol, 2 g), and picolinic acid (20 mmol, 2.46 g) were mixed in a round-bottomed flask (50 mL) in an oil bath. The homogeneous solution was stirred and heated to 110 °C, and after 1 h, the viscous solution was treated with methanol (10 mL, cold). The product (pale yellow solid) was filtered and washed several times with cold methanol.[46] The yield of this reaction was 67% (Scheme S1).

2.2. Synthesis of Complexes PdL_2 and AgL_2. Both complexes were prepared by simple methods as follows:

1. PdL_2: The precise amount of palladium(II) acetate (1 mmol) dissolved in 25 mL of dichloromethane and then 2 mmol of ligand L were added to the solution. The mixture was stirred for 2 h at room temperature and then filtered off.[47] The yield of this reaction was 73%.

2. AgL_2: 2 mmol of L was dissolved in DCM and added to a mixture of AgCl (1 mmol) and ammonia solution (10 mL, 25%) and stirred for 2 h at RT and then filtered off. The yield of this reaction was 58%.

2.3. Preparation of Nanocomposites (rGO@MWCNT/(AgL_2 or PdL_2)@DOX/PEG). Fabrication of nanocomposites started with the addition of 125 mg of MWCNTs to 125 mg of rGO in 20 mL of DI water, and after 30 min of vigorous stirring, the mixture dried out (oven, 70 °C). In the next step, 1 mmol of PdL_2 + 0.5 mmol of DOX and 1 mmol of AgL_2 + 0.5 mmol of DOX were separately added to two different beakers containing 20 mg of rGO@MWCNT, 45 mL of DI water, and 15 mL of ethanol. It is worth mentioning that to prevent DOX's fluorescence quenching, all reactions were conducted in darkness, and all containers were covered with aluminum foil. After 2 h of stirring, 5 mL of PEG-200 was added to the nanocomposites, and after 30 min of stirring, the mixtures were centrifuged (8000 rpm, 10 min) to separate the unbounded

https://doi.org/10.1021/acsomega.3c07432
ACS Omega 2024, 9, 1183−1195

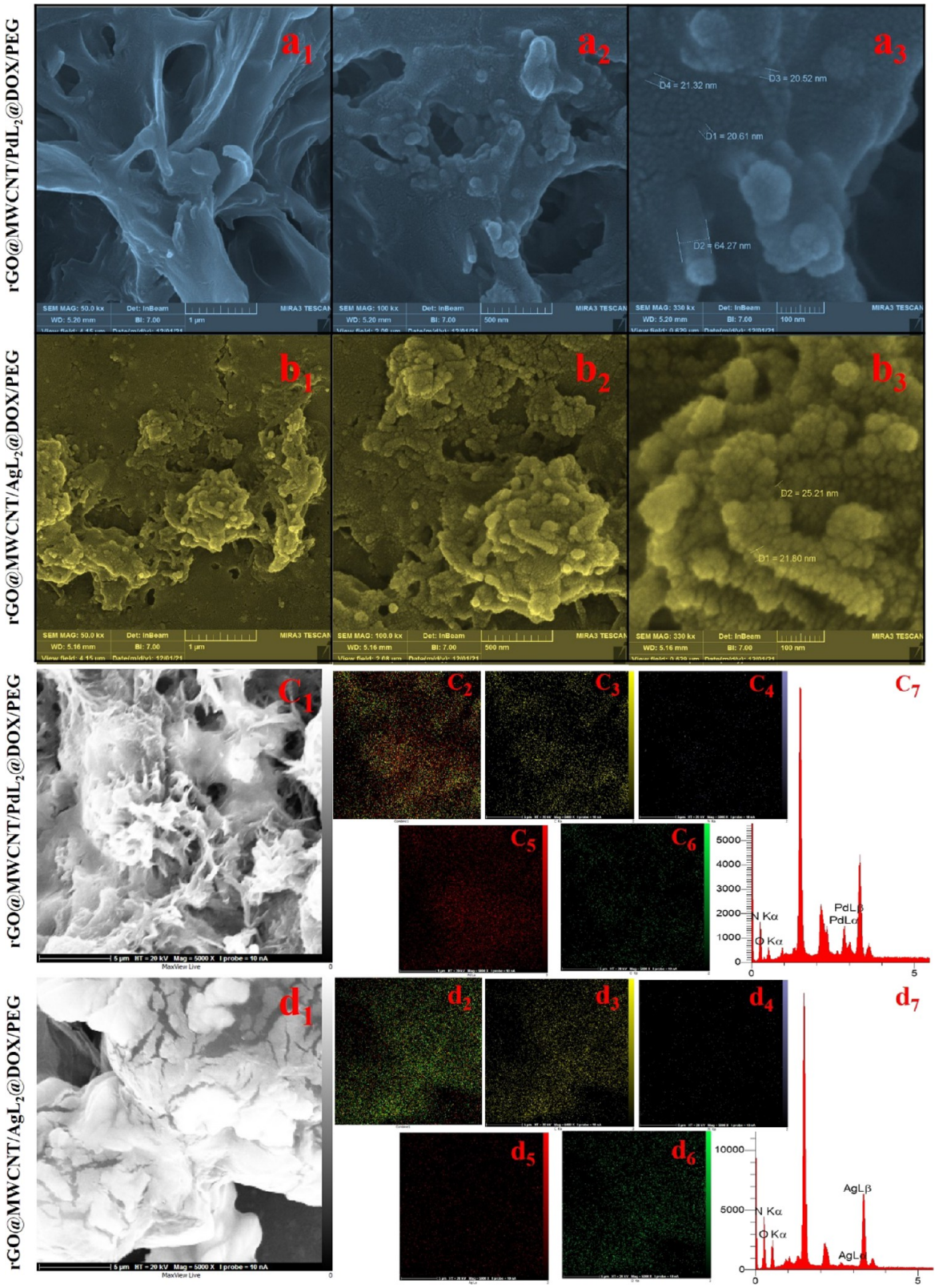

Figure 3. FESEM results of the prepared nanocomposites: (a) rGO@MWCNT/PdL_2@DOX/PEG and (b) rGO@MWCNT/AgL_2@DOX/PEG at various magnifications. EDS and mapping of prepared nanocomposites: (c) rGO@MWCNT/PdL2@DOX/PEG and (d) rGO@MWCNT/AgL_2@DOX/PEG (1, max view; 2, combination; 3, carbon; 4, nitrogen; 5, Pd or Ag; 6, oxygen; 7, energy-dispersive X-ray spectroscopy).

DOX and complexes. The product dried out at room temperature and was kept in a dark place.[47]

2.4. Drug Loading and Release. The delivery ability of the prepared nanocarriers was tested by loading DOX. To this, 5 mg of nanocarriers (rGO@MWCNT/PdL_2 or AgL_2) was sonicated separately (10 min) in 10 mL of DI water, and 1 mg of DOX was added to the mixture in a dark place and stirred for 2 h. The mixture was centrifuged (8000 rpm, 10 min). DOX loading was

https://doi.org/10.1021/acsomega.3c07432
ACS Omega 2024, 9, 1183−1195

investigated utilizing UV−vis spectroscopy.[48] DOX release from prepared nanocomposites was screened at different pH values (phosphate buffer) and 37 °C. Briefly, the precise amount of the prepared compounds was added separately into the buffer solution, and the mixtures were placed in different activated dialysis bags. In the next step, the bags were placed in a PBS buffer at 37 °C and stirred gently in the darkness. At regular intervals, the precise amount of solutions was collected and analyzed.[49]

2.5. Cellular Uptake. In the present study, the MCF-7 and MDA-MB-231 cell lines were seeded in 24-well plates at a density of 1×10^5 cells per well. After 24 h incubation, the medium was replaced with DOX-containing nanocomposites that had been diluted with media several times. In the next step (after 24 h), the treated cells were washed several times with PBS. For the final step, the cells were treated with Hoechst (1 min) and then washed with PBS again and 1 mL of PBS was added to each well.[50]

2.6. Cytotoxicity Assay. The cells were seeded in 96-well plates at a density of 1×10^4 cells per well and incubated with 300 μL of media for a day. Then, the culture medium was replaced with diluted sterilized samples in media and incubated. The well plate medium was changed with culture media containing CCK-8 and again incubated for 1 h. The CCK-8 absorbance was analyzed with a microplate reader.[51]

2.7. XPS. As a proven fact, the C 1s peak can be influenced by various variables, such as crystal orientation, crystalline phase, roughness, or surface cleanness. To achieve a standard and comparable result with other studies, C 1s peak correction should be done. In this regard, the carbon peak correction was done based on assuming 284.8 eV as the reference binding energy.[52]

3. RESULTS AND DISCUSSION

The FT-IR spectra of the prepared nanomaterials have disclosed that all prospective bond peaks appeared in the correct wavenumbers (cm^{-1}) based on the literature. Briefly, the peak at around 3247 cm^{-1} of L is related to the N−H bond, which has vanished in PdL_2 and partially disappeared in AgL_2 due to deprotonation and coordination of the ligand to the metal. There is evidence of the presence of the C−N bond at 1510 cm^{-1}, and for C═Oamidic, there is a sharp peak at about 1594 cm^{-1}. The peak of the C═C stretching mode is demonstrated at around 1650 cm^{-1}. The shift of the $C{=}O_{amidic}$ and C−N peaks in the complex spectra is due to enhancement of the resonance in deprotonated amide (changing the bond strength) and can be another evidence of correct synthesis. All of these peaks are in good agreement with the literature (Figure 2a).[53] Based on the Palai et al. study, the loaded DOX into nanocarriers revealed the characteristic peaks as follows: the band around 1640 cm^{-1} is attributed to DOX's quinone group and the peak near 1350 cm^{-1} corresponds to DOX's $N{-}H_{amidic}$.[54] Also, the broad peak at 3300 cm^{-1} in the composites' spectra is related to the O−H bond and the intensity of this peak in PEGylated nanocomposites is higher; it is clear that the presence of PEG on the surface of the prepared nanocomposites has literally covered the peaks of other compounds (Figure 2b). The UV−vis spectra of fabricated nanomaterials were collected in DCM (Figure S2). The ligand's band (L) is demonstrated at about 220 and 293 nm, which are assigned to the $\pi \rightarrow \pi^*$ (aromatic rings) and $n \rightarrow \pi^*$ (electron pair of nitrogen) intraligand transitions, respectively. PdL_2's broad bands are centered at around 245 and 322 nm and are related to intraligand transitions and charge transfer. AgL_2's peaks appear at 278 nm and near 230 nm. Change in the peak position can be reliable evidence of coordination of L to Pd or Ag.[55]

The X-ray photoelectron spectroscopy (XPS) survey confirmed the presence of metals in the structures (Figure 2d). The most sensitive and important part of XPS data analysis would be correct peak fitting; this fitting has been done carefully and is reported in Figure 2e−g. Although the broadness or height of subpeaks can indicate different chemical and electronic phenomena, the main ordeal is that XPS peaks' shape can be influenced by various factors like inelastic scattering, charging effects, satellite peaks, and instrumental broadening. All in all, as a scientific fact, taller subpeaks can demonstrate stronger interactions and higher concentrations of particular chemical states, while broader subpeaks illustrate spread binding energy (different environments or molecular configurations of the same chemical state), chemical variation (different molecular interactions, oxidation states, or coordination environments), and disorder of structures (various molecular conformations). Accordingly, the fitted N 1s subpeaks of L revealed that all three moieties are in their right positions, and their element percentages are near each other. As the fitted subpeaks of PdL_2 and AgL_2 demonstrate, the element's percentage has changed considerably, which is one of the signs of coordination of the ligand to the metal. Based on these data, palladium may be connected to $N_{pyridine}$ and N_{amide} for three reasons; the first one can be the considerable height of $N_{pyridine}$, the second would be the 0.2316 eV shift of N_{amide}, and the third one is the broadening of $N_{thiazole}$. On the other side of the coin, silver may mainly coordinate with Npyridine and $N_{thiazole}$ instead of N_{amide}. This hypothesis comes from a sharper $N_{thiazole}$ subpeak and more shift in comparison with N_{amide}. This can be owing to the fact that palladium is smaller than silver.

The L, PdL_2, and AgL_2 ^1H NMR spectra were measured in deuterated solvents and are shown in Figure 2c and Figure S1. The broad peak of amidic protons (N−H) can be the most important in compounds with a carboxamide functional group because this peak will vanish after the coordination of N_{amide} to the metal. As can be seen in Figure 2c, the abovementioned peak appeared at 11.94 ppm and this peak disappeared after complexation with palladium and silver. The broad peak at around 11.3 ppm could be related to N_{amide}, which has been shifted, or as a proven fact, sometimes and after complexation, the peak of hydrogen of carbon next to pyridine comes to the downfield. The hydrogens of the thiazole ring (H_b and H_c) can be observed as two doublet peaks at 7.59 and 7.37 ppm, respectively. The peaks at around 7.72−8.78 ppm are attributed to the pyridine ring's hydrogen.[56]

The nanostructure morphology can be examined by field emission scanning electron microscopy (FESEM). As can be seen in Figure 3a,b, the cylindrical structures of the MWCNTs and rGO sheets are vividly observable. The presence of PdL_2/AgL_2, DOX, and PEG led to moderate aggregation.[57] The other useful analysis for screening the components' distribution on the nanocarriers and their proportion is energy-dispersive X-ray spectroscopy (EDS). The prepared nanocomposites' chemical composition is demonstrated in Figure 3c,d. The presence of the prepared complexes on the nanocomposites is confirmed by this analysis. The collected results demonstrate that all elements are well distributed and are in good agreement with the reagents' ratio.

In order to get insight, transmission electron microscopy (TEM) images were taken and are shown in Figure 4. Various

https://doi.org/10.1021/acsomega.3c07432
ACS Omega 2024, 9, 1183−1195

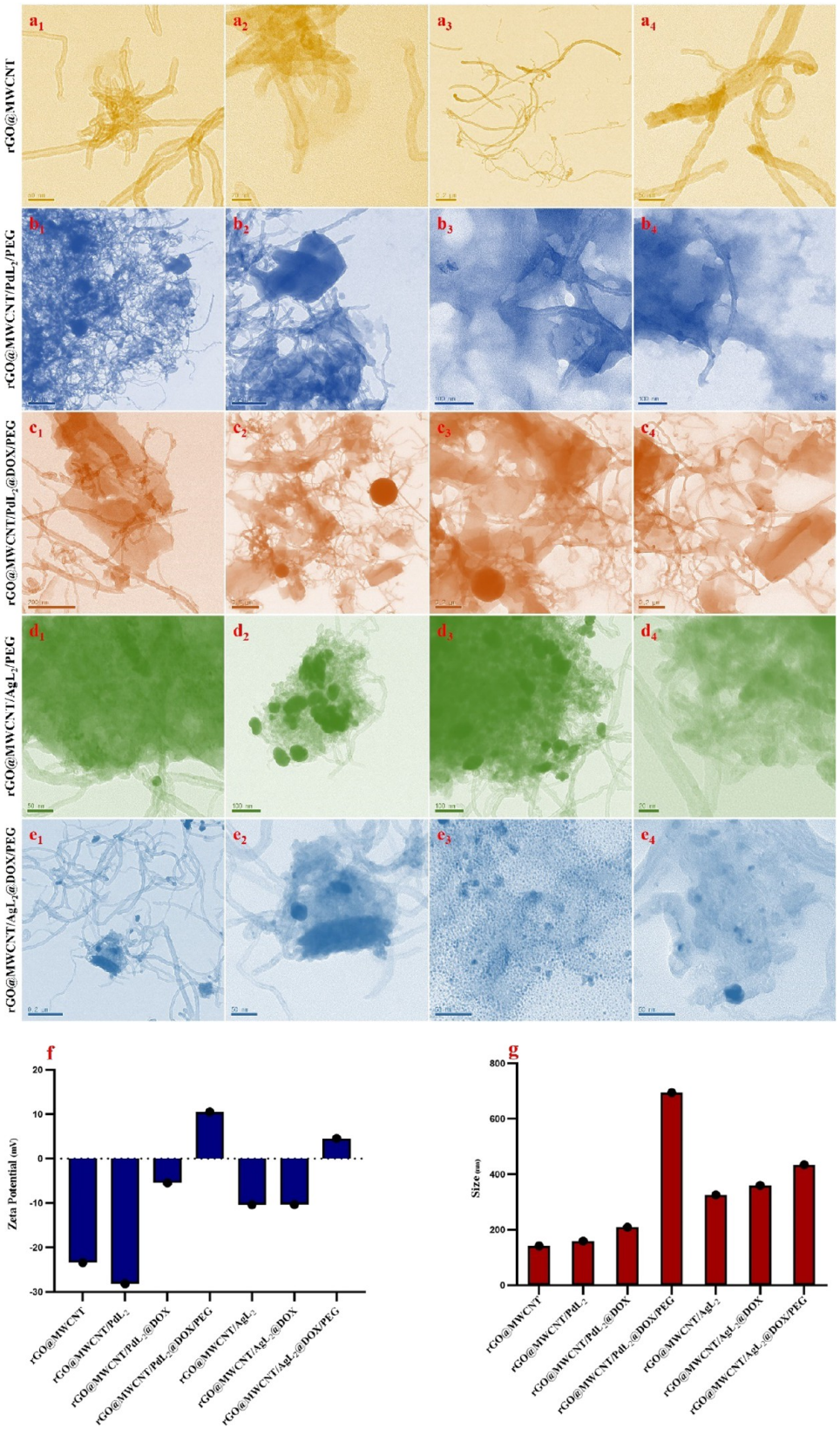

Figure 4. TEM results of the prepared nanocomposites: (a) rGO@MWCNT, (b) (rGO@MWCNT/PdL_2/PEG), (c) (rGO@MWCNT/PdL_2@DOX/PEG), (d) (rGO@MWCNT/AgL_2/PEG), and (e) (rGO@MWCNT/AgL_2@DOX/PEG); (f) zeta potential of the prepared compounds; and (g) DLS of the fabricated nanocompounds.

magnifications of the prepared nanocompounds demonstrated that all materials are evenly distributed on the surface of the nanocarrier, and their presence can be seen vividly. Based on the TEM images, the presence of rGO and MWCNTs from the size

https://doi.org/10.1021/acsomega.3c07432
ACS Omega 2024, 9, 1183−1195

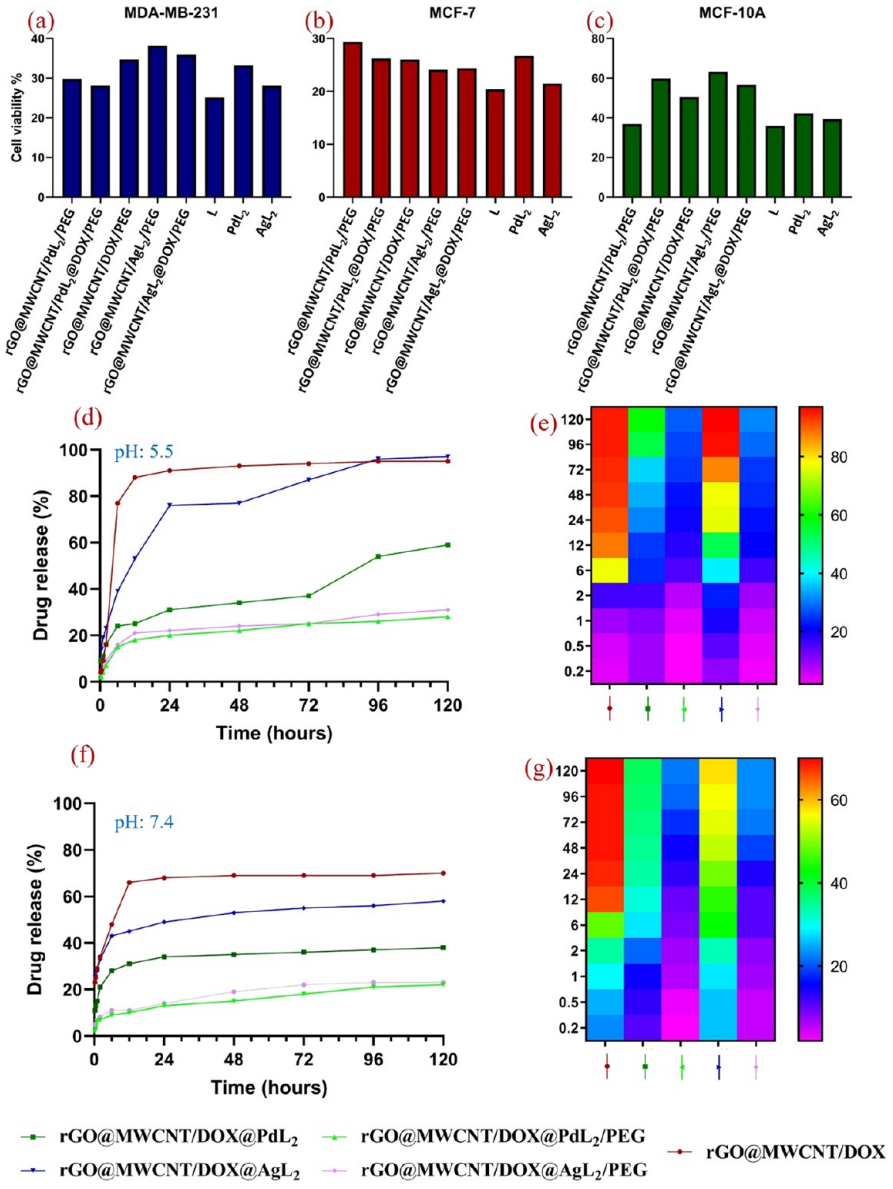

Figure 5. Cytotoxicity assay after 24 h treatment of high concentrations of rGO@MWCNT/PdL_2/PEG, rGO@MWCNT/PdL_2@DOX/PEG, rGO@MWCNT/DOX/PEG, rGO@MWCNT/AgL_2/PEG, and rGO@MWCNT/AgL_2@DOX/PEG, L, PdL_2, and AgL_2 on the (a) MDA-MB-231, (b) MCF-7, and (c) MCF-10A cell lines. The characteristic time- and pH-dependent drug release profiles of the prepared nanocomposites at pH 5.5 and 7.4 are demonstrated in (d) and (f), respectively. The 2D heat maps of the drug release profiles at pH 5.5 and 7.4 are illustrated in (e) and (g), respectively.

and length of 10 nm is observable. The average size of nanocompounds is screened without filtration and is reported in Figure 4g. Based on the DLS results, the addition of AgL_2 or PdL_2 led to slightly increasing the size of the nanocarrier and the addition of DOX and complexes (AgL_2 or PdL_2) simultaneously to the nanocarrier led to a higher compound size. The highest size is related to the PEGylated nanocompounds. and increase of the size after PEGylation is a proven fact and is changeable by changing PEG's amount and molecular weight. Although the particle size of PEGylated nanocompounds is larger than that of non-PEGylated nanocompounds, other studies disclosed that PEGylation leads to a longer circulation lifetime and lower capturing by the lung, spleen, and liver[58]; reduces immunogenicity; and boosts permeability and retention time in tumor.[59] Bozuyuk et al. studied the various factors of PEGylation for the size and zeta potential of final compounds. As a result of their study, changing PEG's molecular weight and ratio and the pH of the solution can change the size of the final compound[60] but size optimization was not the aim of this study. The surface charges of the prepared nanocomposites were screened and are reported in Figure 4f. The results demonstrated that the surface charge of the rGO@MWCNT nanocarrier is negative and PEGylation led to the zeta potential increasing and reaching a positive surface charge. Based on the Kouchakzadeh et al. study, PEGylation has a significant impact on surface charge and can increase it.[59] Long et al. studied various lengths of MWCNTs and reported that smaller MWCNTs have a neutral zeta potential, but longer MWCNTs have negative charges. Also, they studied MWCNT internalization into the mitochondria and nuclei of cells and reported that although MWCNTs revealed good penetration, longer MWCNTs led to intracellular vacuolation and membrane damage.[61]

https://doi.org/10.1021/acsomega.3c07432
ACS Omega 2024, 9, 1183−1195

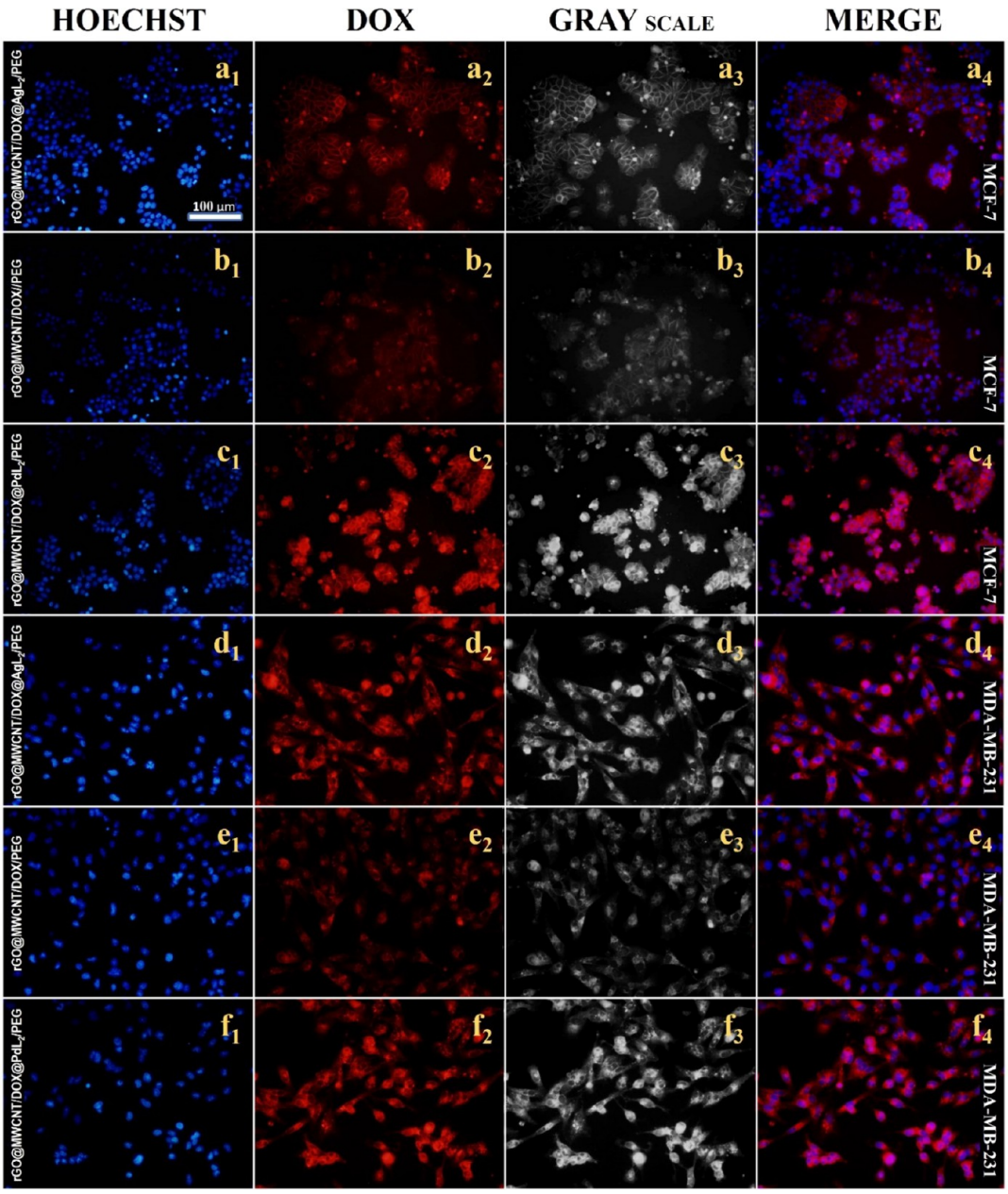

Figure 6. Images of intracellular uptake of DOX by 2D fluorescence microscopy, (a, d) (rGO@MWCNT/AgL_2@DOX/PEG), (b, e) (rGO@MWCNT/DOX/PEG), and (c, f) (rGO@MWCNT/PdL_2@DOX/PEG), on two different cell lines: MCF-7 and MDA-MB-231.

3.1. Cytotoxicity Assay. The prepared nanomaterials' biocompatibility was assessed with Cell Counting Kit-8 against various cancerous and normal breast cell lines (MCF-10A, MCF-7, and MDA-MB-231). Cell viability was investigated with a high concentration (2000 μg/mL) of the prepared compounds after 24 h. As shown in Figure 5, the most cytotoxic compound was L, which showed the highest cytotoxicity to all cell lines. The assessed cytotoxicity of the prepared complexes revealed that AgL_2 is more cytotoxic than PdL_2 (~5%), which might be related to the ability of AgL_2 to prepare more ROS. Based on the CCK-8 assay results, the most important point of this investigation was the higher cell viability for both the final compounds (rGO@MWCNT/PdL_2@DOX/PEG and rGO@MWCNT/AgL_2@DOX/PEG) of the normal cell line (MCF-10A) compared to the high cytotoxicity to the cancerous cell lines (MDA-MB-231 and MCF-7), which are quite promising in the anticancer and drug delivery field. The dose-dependent response of this kind of prepared carbon-based nanomaterial and nanocomposite was reported in our group's previous papers, and because of that, the aim of this study was not optimization; we just performed high-concentration cytotoxicity assessment to understand the maximum differences between the prepared compounds. The collected data demonstrate that the fabricated nanocomposites (rGO@MWCNT/AgL_2@DOX/PEG and rGO@MWCNT/PdL_2@DOX/PEG) had high cytotoxicity to cancerous cells and high biocompatibility with the normal cell line, which proved that utilizing the complexes with DOX is promising and applicable.

3.2. Drug Release. As a scientific fact, the microenvironment of tumorous cells is acidic, and their pH value is about one unit lower than that of normal cells. The *in vitro* drug release behavior of DOX-containing compounds has been studied in

https://doi.org/10.1021/acsomega.3c07432
ACS Omega 2024, 9, 1183−1195

different pH environments (5.5 and 7.4). Figure 5 presents the initial high rate of release (burst phase) from the nanocarriers for all prepared compounds, and this would be due to the easy protonation of DOX, which is weakly connected to the surface of nanocarriers (adsorbed), and protonation of DOX leads to increasing DOX's solubility. This phenomenon is more drastic when only DOX is loaded into the nanocarrier, and as can be seen, the presence of carboxamide-based complexes decreased the release rate of DOX in both acidic and physiological pH environments. As a proven fact, addition of PEG will decrease the release of DOX from nanocarriers. Ghaferi et al. reported that their PEGylated nanocarriers demonstrated about 20% less DOX release.[62] In this study, both PEGylated nanocarriers behaved in the same manner, which means that PEG completely covered the loaded nanocarriers. Comparison of the release profiles of rGO@MWCNT/DOX in acidic and physiological pH discloses that the DOX release from the nondecorated and noncoated nanocarrier hit the top value before the first 12 h and after that it plateaued (the DOX release was about 35% more in acidic pH in comparison with that in physiological pH). Analysis of the collected data on rGO@MWCNT/PdL_2@DOX and rGO@MWCNT/AgL_2@DOX in pH 7.4 showed that utilizing PdL_2 led to an about 45% decrease in drug release. The simulated acidic pH increased the amount of released DOX from rGO@MWCNT/AgL_2@DOX, whereas the DOX release behavior from rGO@MWCNT/PdL_2@DOX was the same as its release at pH 7.4 during the first 72 h. Acidic pH had negligible impact on the total amount of released DOX from PEGylated compounds but led to reaching the maximum value faster than that in physiological pH. This study's results are in good agreement with previous studies; combining carboxamide-based complexes with DOX led to increasing the stability and sustained release of DOX. The examined compounds revealed pH-dependent sustained release, which suggests them as a reliable candidate for drug/gene delivery applications because they can release therapeutic agents surely and slowly.[63]

3.3. Drug Internalization. DOX resistance is increasing too fast, and although its exact mechanism is not proven, scientists proposed two probable mechanisms, (i) decreasing the P-glycoprotein population that are responsible for transferring and gathering DOX inside cells and (ii) increasing the B-cell lymphoma 2, which is an antiapoptotic agent.[64] As a proven fact, utilizing carbon-based carriers can address this issue by effectively connecting to the cell membrane.[65] Cellular uptake can happen through different mechanisms like endocytosis-independent or passive diffusion. The presence of endocytosis inhibitors will make cell penetration completely low. The best technique for tracking DOX internalization is using a special kind of microscope like a CLSM or a 2D fluorescence microscope. The images in Figure 6 disclose that DOX passes through the cell membrane effectively and aggregates inside the cells. The grayscale images can show the cells' morphology. The merged images confirm the precise internalization of nanocomposites and release DOX site-specifically. The cell population when the nanocomposites do not consist of AgL_2 or PdL_2 is lower than that for complex-containing nanocomposites, and also the DOX intensity in complex-containing nanocomposites is vividly higher than that in rGO@MWCNT/DOX/PEG. Debnath and Srivastava disclosed that carbon-based nanocomposites can penetrate into cells through both endocytosis-independent and passive diffusion mechanisms. Also, based on their study, one of the main factors of efficient cellular uptake is carrier surface charge.[66] PEGylation has increased the surface charge of the final nanocomposites; the considerable intensity of DOX inside the cells can be due to the better interaction of the cell membrane with nanocomposites.

4. CONCLUSIONS

New vistas have been opened in the field of cancer therapy through bioengineering and developing nanocompounds. Carbon-based nanocarriers are quite well-known among scientists owing to their surface functionalizability, large surface area, near-infrared absorption, small size, and bioactivity. Carboxamide-based silver and palladium complexes adorned on the nanocarriers owing to their unique properties can control infection and stabilize DOX on the nanocarriers, and the whole structure was PEGylated to lower the cytotoxicity. rGO@MWCNT/PdL_2@DOX/PEG and rGO@MWCNT/AgL_2@DOX/PEG were fabricated, and their biomedical applicability was screened *in vitro* (MDA-MB-231, MCF-7, and MCF-10A). The CCK-8 assay results revealed that decorating PdL_2 beside DOX on the carbon-based nanocarriers not only led to higher cell viability of the normal cell line (in comparison with that for the AgL_2-containing nanocarrier) but also increased the cytotoxicity against cancerous cell lines. In addition, the drug release investigations revealed that adorning the carbon-based nanocarriers with PdL_2 and AgL_2 will lead to preclusion of spontaneous release and the presence of PdL_2 on the DOX-containing nanocarrier could decrease DOX release (by about 45%) compared to the AgL_2-containing nanocomposite. At the end, both PEGylated loaded nanocarriers revealed the same DOX release behavior in acidic and physiological pH.

■ ASSOCIATED CONTENT

Supporting Information

The Supporting Information is available free of charge at https://pubs.acs.org/doi/10.1021/acsomega.3c07432.

Ligand's synthesis scheme, ^{1}H NMR spectra of the ligand and complexes, and UV−vis spectra of the ligand and complexes (PDF)

■ AUTHOR INFORMATION

Corresponding Authors

Mojtaba Bagherzadeh − *Department of Chemistry, Sharif University of Technology, Tehran 11155-9465, Iran;* orcid.org/0000-0003-3009-3693; Email: bagherzadeh@sharif.edu

Yun Suk Huh − *NanoBio High-Tech Materials Research Center, Department of Biological Sciences and Bioengineering, Inha University, Incheon 402-751, Republic of Korea;* orcid.org/0000-0003-1612-4473; Email: yunsuk.huh@inha.ac.kr

Authors

Moein Safarkhani − *NanoBio High-Tech Materials Research Center, Department of Biological Sciences and Bioengineering, Inha University, Incheon 402-751, Republic of Korea; Department of Chemistry, Sharif University of Technology, Tehran 11155-9465, Iran;* orcid.org/0000-0001-7062-073X

Sadaf Saboori Moghaddam − *Department of Chemistry, University of Milano, 20133 Milan, Italy*

Fahimeh Taghavimandi − *NanoBio High-Tech Materials Research Center, Department of Biological Sciences and*

https://doi.org/10.1021/acsomega.3c07432
ACS Omega 2024, 9, 1183−1195

Bioengineering, Inha University, Incheon 402-751, Republic of Korea

Yousef Fatahi − *Nanotechnology Research Centre, Faculty of Pharmacy and Department of Pharmaceutical Nanotechnology, Faculty of Pharmacy, Tehran University of Medical Sciences, Tehran 1416753955, Iran; Universal Scientific Education and Research Network (USERN), Tehran 1416753955, Iran;* orcid.org/0000-0003-0374-2141

Uichang Park − *NanoBio High-Tech Materials Research Center, Department of Biological Sciences and Bioengineering, Inha University, Incheon 402-751, Republic of Korea*

Fatemeh Radmanesh − *Uro-Oncology Research Center, Tehran University of Medical Sciences, Tehran 1416753955, Iran; Department of Stem Cells and Developmental Biology, Cell Science Research Center, Royan Institute for Stem Cell Biology and Technology, ACECR, Tehran 16635-14, Iran*

Navid Rabiee − *School of Engineering, Macquarie University, Sydney, New South Wales 2109, Australia;* orcid.org/0000-0002-6945-8541

Complete contact information is available at: https://pubs.acs.org/10.1021/acsomega.3c07432

Author Contributions

Conceptualization, M.S. and N.R.; methodology, U.P., F.T., and F.R.; investigation, M.S. and S.S.M.; resources, M.B. and Y.H.; data curation and writing—original draft preparation, M.S. and S.S.M; writing—review and editing, N.R., Y.H., and M.B.; visualization, Y.F. All authors have read and agreed to publish this version of the manuscript.

Notes

The authors declare no competing financial interest.

■ ACKNOWLEDGMENTS

This work was supported by the Basic Science Research Program through the National Research Foundation of Korea (NRF-2021R1A2C3011585 and 2022M3J7A1062940) funded by the Ministry of Science, ICT and Future Planning (MSIP), Republic of Korea. Support of this study by the Inha University and Sharif University of Technology Research Councils is gratefully acknowledged.

■ REFERENCES

(1) Chatterjee, A.; Mambo, E.; Sidransky, D. Mitochondrial DNA mutations in human cancer. *Oncogene* **2006**, *25* (34), 4663−4674.

(2) Kalyanaraman, B. Teaching the basics of cancer metabolism: Developing antitumor strategies by exploiting the differences between normal and cancer cell metabolism. *Redox biology* **2017**, *12*, 833−842.

(3) Woodhouse, E. C.; Chuaqui, R. F.; Liotta, L. A. General mechanisms of metastasis. *Cancer* **1997**, *80* (S8), 1529−1537.

(4) Schuster, M.; Nechansky, A.; Kircheis, R. Cancer immunotherapy. *Biotechnology Journal: Healthcare Nutrition Technology* **2006**, *1* (2), 138−147.

(5) DeVita, V. T., Jr.; Chu, E. A history of cancer chemotherapy. *Cancer research* **2008**, *68* (21), 8643−8653.

(6) Rastelli, F.; Crispino, S. Factors predictive of response to hormone therapy in breast cancer. *Tumori Journal* **2008**, *94* (3), 370−383.

(7) Schaue, D.; McBride, W. H. Opportunities and challenges of radiotherapy for treating cancer. *Nature reviews Clinical oncology* **2015**, *12* (9), 527−540.

(8) Avramović, N.; Mandić, B.; Savić-Radojević, A.; Simić, T. Polymeric nanocarriers of drug delivery systems in cancer therapy. *Pharmaceutics* **2020**, *12* (4), 298.

(9) Moghaddam, F. D.; Heidari, G.; Zare, E. N.; Djatoubai, E.; Paiva-Santos, A. C.; Bertani, F. R.; Wu, A. Carbohydrate polymer-based nanocomposites for breast cancer treatment. *Carbohydr. Polym.* **2022**, *304*, No. 120510.

(10) Dai, X.; Cheng, H.; Bai, Z.; Li, J. Breast cancer cell line classification and its relevance with breast tumor subtyping. *Journal of Cancer* **2017**, *8* (16), 3131.

(11) Al-Hajj, M.; Wicha, M. S.; Benito-Hernandez, A.; Morrison, S. J.; Clarke, M. F. Prospective identification of tumorigenic breast cancer cells. *Proc. Natl. Acad. Sci. U. S. A.* **2003**, *100* (7), 3983−3988.

(12) Schirrmacher, V. From chemotherapy to biological therapy: A review of novel concepts to reduce the side effects of systemic cancer treatment. *International journal of oncology* **2018**, *54* (2), 407−419.

(13) Edis, Z.; Wang, J.; Waqas, M. K.; Ijaz, M.; Ijaz, M. Nanocarriers-mediated drug delivery systems for anticancer agents: An overview and perspectives. *Int. J. Nanomed.* **2021**, *16*, 1313.

(14) Hossen, S.; Hossain, M. K.; Basher, M.; Mia, M.; Rahman, M.; Uddin, M. J. Smart nanocarrier-based drug delivery systems for cancer therapy and toxicity studies: A review. *Journal of advanced research* **2019**, *15*, 1−18.

(15) Yetisgin, A. A.; Cetinel, S.; Zuvin, M.; Kosar, A.; Kutlu, O. Therapeutic nanoparticles and their targeted delivery applications. *Molecules* **2020**, *25* (9), 2193.

(16) Gupta, N.; Bhagat, S.; Singh, M.; Jangid, A. K.; Bansal, V.; Singh, S.; Pooja, D.; Kulhari, H. Site-specific delivery of a natural chemotherapeutic agent to human lung cancer cells using biotinylated 2D rGO nanocarriers. *Materials Science and Engineering: C* **2020**, *112*, No. 110884.

(17) Vargason, A. M.; Anselmo, A. C.; Mitragotri, S. The evolution of commercial drug delivery technologies. *Nature Biomedical Engineering* **2021**, *5* (9), 951−967.

(18) Wu, J. The enhanced permeability and retention (EPR) effect: the significance of the concept and methods to enhance its application. *Journal of Personalized Medicine* **2021**, *11* (8), 771.

(19) Narvekar, M.; Xue, H. Y.; Eoh, J. Y.; Wong, H. L. Nanocarrier for poorly water-soluble anticancer drugs—barriers of translation and solutions. *Aaps Pharmscitech* **2014**, *15* (4), 822−833.

(20) Savjani, K. T.; Gajjar, A. K.; Savjani, J. K. Drug solubility: importance and enhancement techniques. *Int. Scholarly Res. Not.* **2012**, *2012*, No. 195727.

(21) Ashrafizadeh, M.; Saebfar, H.; Gholami, M. H.; Hushmandi, K.; Zabolian, A.; Bikarannejad, P.; Hashemi, M.; Daneshi, S.; Mirzaei, S.; Sharifi, E.; Kumar, A. P.; Khan, H.; Hossein, H. H. S.; Vosough, M.; Rabiee, N.; Thakur, V. K.; Makvandi, P.; Mishra, Y. K.; Tay, F. R.; Wang, Y.; Zarrabi, A.; Orive, G.; Mostafavi, E. Doxorubicin-loaded graphene oxide nanocomposites in cancer medicine: Stimuli-responsive carriers, co-delivery and suppressing resistance. *Expert Opin. Drug Delivery* **2022**, *19* (4), 355−382.

(22) Mirza-Aghayan, M.; Heidarian, M.; Mohammadi, M.; Boukherroub, R. Synthesis and characterization of a novel multi-functionalized reduced graphene oxide as a pH-sensitive drug delivery material and a photothermal candidate. *Appl. Surf. Sci.* **2022**, *583*, No. 152568.

(23) Majhi, S. M.; Mirzaei, A.; Kim, H. W.; Kim, S. S. Reduced graphene oxide (rGO)-loaded metal-oxide nanofiber gas sensors: An overview. *Sensors* **2021**, *21* (4), 1352.

(24) Huda, S.; Alam, M. A.; Sharma, P. K. Smart nanocarriers-based drug delivery for cancer therapy: An innovative and developing strategy. *Journal of Drug Delivery Science and Technology* **2020**, *60*, No. 102018.

(25) Cheon, J.; Cho, D. Effect of MWCNT anchoring to the carbon fiber surface on the interlaminar property and fracture topography of carbon fabric/vinyl ester composites: comparisons between conventional and semi-spread carbon fabrics. *Carbon Lett.* **2023**, 1−8.

(26) Bhattacharya, K.; Mukherjee, S. P.; Gallud, A.; Burkert, S. C.; Bistarelli, S.; Bellucci, S.; Bottini, M.; Star, A.; Fadeel, B. Biological interactions of carbon-based nanomaterials: From coronation to degradation. *Nanomedicine: Nanotechnology, Biology and Medicine* **2016**, *12* (2), 333−351.

(27) Karimi-Maleh, H.; Alizadeh, M.; Orooji, Y.; Karimi, F.; Baghayeri, M.; Rouhi, J.; Tajik, S.; Beitollahi, H.; Agarwal, S.; Gupta, V. K.; Rajendran, S.; Rostamnia, S.; Fu, L.; Saberi-Movahed, F.;

Malekmohammadi, S. Guanine-based DNA biosensor amplified with Pt/SWCNTs nanocomposite as analytical tool for nanomolar determination of daunorubicin as an anticancer drug: a docking/experimental investigation. *Ind. Eng. Chem. Res.* **2021**, *60* (2), 816−823.
(28) Murjani, B. O.; Kadu, P. S.; Bansod, M.; Vaidya, S. S.; Yadav, M. D. Carbon nanotubes in biomedical applications: current status, promises, and challenges. *Carbon Letters* **2022**, *32* (5), 1207−1226.
(29) Klinger, D.; Landfester, K. Stimuli-responsive microgels for the loading and release of functional compounds: Fundamental concepts and applications. *Polymer* **2012**, *53* (23), 5209−5231.
(30) Marloye, M.; Berger, G.; Gelbcke, M.; Dufrasne, F. A survey of the mechanisms of action of anticancer transition metal complexes. *Future medicinal chemistry* **2016**, *8* (18), 2263−2286.
(31) Arteaga, C. L.; Johnson, D. H. Tyrosine kinase inhibitors—ZD1839 (Iressa). *Current opinion in oncology* **2001**, *13* (6), 491−498.
(32) Pokrywka, A.; Cholbinski, P.; Kaliszewski, P.; Kowalczyk, K.; Konczak, D.; Zembron-Lacny, A. Metabolic modulators of the exercise response: doping control analysis of an agonist of the peroxisome proliferator-activated receptor δ (GW501516) and 5-aminoimidazole-4-carboxamide ribonucleotide (AICAR). *J. Physiol. Pharmacol.* **2014**, *65* (4), 469−476.
(33) Manam, N.; Harun, W.; Shri, D.; Ghani, S.; Kurniawan, T.; Ismail, M. H.; Ibrahim, M. Study of corrosion in biocompatible metals for implants: A review. *J. Alloys Compd.* **2017**, *701*, 698−715.
(34) Fenton, O. S.; Olafson, K. N.; Pillai, P. S.; Mitchell, M. J.; Langer, R. Advances in biomaterials for drug delivery. *Adv. Mater.* **2018**, *30* (29), No. 1705328.
(35) Javanbakht, S.; Shaabani, A. Multicomponent reactions-based modified/functionalized materials in the biomedical platforms. *ACS Applied Bio Materials* **2020**, *3* (1), 156−174.
(36) Aghazadeh Tabrizi, M.; Baraldi, P. G.; Baraldi, S.; Gessi, S.; Merighi, S.; Borea, P. A. Medicinal chemistry, pharmacology, and clinical implications of TRPV1 receptor antagonists. *Medicinal research reviews* **2017**, *37* (4), 936−983.
(37) Veinberg, G.; Vavers, E.; Orlova, N.; Kuznecovs, J.; Domracheva, I.; Vorona, M.; Zvejniece, L.; Dambrova, M. Stereochemistry of phenylpiracetam and its methyl derivative: improvement of the pharmacological profile. *Chem. Heterocycl. Compd.* **2015**, *51* (7), 601−606.
(38) Micallef, I.; Baron, B. Doxorubicin: An overview of the anti-cancer and chemoresistance mechanisms. *Ann. Clin. Toxicol.* **2020**, *3* (2), 1031.
(39) Van't Veer, L. J.; Bernards, R. Enabling personalized cancer medicine through analysis of gene-expression patterns. *Nature* **2008**, *452* (7187), 564−570.
(40) Taylor-Papadimitriou, J.; Burchell, J.; Miles, D.; Dalziel, M. MUC1 and cancer. *Biochimica et Biophysica Acta (BBA)-Molecular Basis of Disease* **1999**, *1455* (2−3), 301−313.
(41) Mishra, P.; Nayak, B.; Dey, R. PEGylation in anti-cancer therapy: An overview. *Asian journal of pharmaceutical sciences* **2016**, *11* (3), 337−348.
(42) Suk, J. S.; Xu, Q.; Kim, N.; Hanes, J.; Ensign, L. M. PEGylation as a strategy for improving nanoparticle-based drug and gene delivery. *Advanced drug delivery reviews* **2016**, *99*, 28−51.
(43) Farace, C.; Sánchez-Moreno, P.; Orecchioni, M.; Manetti, R.; Sgarrella, F.; Asara, Y.; Peula-García, J. M.; Marchal, J. A.; Madeddu, R.; Delogu, L. G. Immune cell impact of three differently coated lipid nanocapsules: pluronic, chitosan and polyethylene glycol. *Sci. Rep.* **2016**, *6* (1), 18423.
(44) D'souza, A. A.; Shegokar, R. Polyethylene glycol (PEG): a versatile polymer for pharmaceutical applications. *Expert opinion on drug delivery* **2016**, *13* (9), 1257−1275.
(45) Juhás, M.; Bachtíková, A.; Nawrot, D. E.; Hatoková, P.; Pallabothula, V. S. K.; Diepoltová, A.; Jand'ourek, O.; Bárta, P.; Konečná, K.; Paterová, P.; Šesták, V.; Zitko, J. Improving antimicrobial activity and physico-chemical properties by isosteric replacement of 2-aminothiazole with 2-aminooxazole. *Pharmaceuticals* **2022**, *15* (5), 580.
(46) Kiani, M.; Bagherzadeh, M.; Meghdadi, S.; Fadaei-Tirani, F.; Babaie, M.; Schenk-Joss, K. Synthesis, characterisation and crystal structure of a new Cu (II)-carboxamide complex and CuO nanoparticles as new catalysts in the CuAAC reaction and investigation of their antibacterial activity. *Inorg. Chim. Acta* **2020**, *506*, No. 119514.
(47) Bagherzadeh, M.; Safarkhani, M.; Kiani, M.; Radmanesh, F.; Daneshgar, H.; Ghadiri, A. M.; Taghavimandi, F.; Fatahi, Y.; Safari-Alighiarloo, N.; Ahmadi, S.; Rabiee, N. MIL-125-based nanocarrier decorated with Palladium complex for targeted drug delivery. *Sci. Rep.* **2022**, *12* (1), 12105.
(48) Zhang, Z.; Lei, Y.; Yang, X.; Shi, N.; Geng, L.; Wang, S.; Zhang, J.; Shi, S. High drug-loading system of hollow carbon dots−doxorubicin: preparation, in vitro release and pH-targeted research. *J. Mater. Chem. B* **2019**, *7* (13), 2130−2137.
(49) Radmansouri, M.; Bahmani, E.; Sarikhani, E.; Rahmani, K.; Sharifianjazi, F.; Irani, M. Doxorubicin hydrochloride-Loaded electrospun chitosan/cobalt ferrite/titanium oxide nanofibers for hyperthermic tumor cell treatment and controlled drug release. *Int. J. Biol. Macromol.* **2018**, *116*, 378−384.
(50) Qiu, L.; Xu, J.; Ahmed, K. S.; Zhu, M.; Zhang, Y.; Long, M.; Chen, W.; Fang, W.; Zhang, H.; Chen, J. Stimuli-responsive, dual-function prodrug encapsulated in hyaluronic acid micelles to overcome doxorubicin resistance. *Acta Biomaterialia* **2022**, *140*, 686−699.
(51) Jiao, G.; He, X.; Li, X.; Qiu, J.; Xu, H.; Zhang, N.; Liu, S. Limitations of MTT and CCK-8 assay for evaluation of graphene cytotoxicity. *Rsc Advances* **2015**, *5* (66), 53240−53244.
(52) Greczynski, G.; Hultman, L. The same chemical state of carbon gives rise to two peaks in X-ray photoelectron spectroscopy. *Sci. Rep.* **2021**, *11* (1), 11195.
(53) Bagherzadeh, M.; Safarkhani, M.; Daneshgar, H.; Radmanesh, F.; Taghavimandi, F.; Ghadiri, A. M.; Kiani, M.; Fatahi, Y.; Safari-Alighiarloo, N.; Ahmadi, S.; Rabiee, N. Magnetic carbon−based nanocomposite decorated with palladium complex for co-delivery of DOX/pCRISPR. *J. Drug Delivery Sci. Technol.* **2022**, *78*, No. 103917.
(54) Palai, P. K.; Mondal, A.; Chakraborti, C. K.; Banerjee, I.; Pal, K.; Rathnam, V. S. S. Doxorubicin loaded green synthesized nanoceria decorated functionalized graphene nanocomposite for cancer-specific drug release. *Journal of Cluster Science* **2019**, *30*, 1565−1582.
(55) Omura, G.; Major, F.; Blessing, J.; Sedlacek, T.; Thigpen, J.; Creasman, W.; Zaino, R. A randomized study of adriamycin with and without dimethyl triazenoimidazole carboxamide in advanced uterine sarcomas. *Cancer* **1983**, *52* (4), 626−632.
(56) Kiani, M.; Bagherzadeh, M.; Meghdadi, S.; Fadaei-Tirani, F.; Babaie, M.; Schenk-Joß, K. Promising new catalytic properties of a Co (II)-carboxamide complex and its derived Co3O4 nanoparticles for the Mizoroki-Heck and the Epoxidation reactions. *Appl. Organomet. Chem.* **2020**, *34* (11), No. e5911.
(57) Reddy, M. S. B.; Kailasa, S.; Rani, B. G.; Munindra, P.; Bikshalu, K.; Rao, K. V. CeO2 nano-hexagons decorated rGO/CNT heterostructure for high-performance LPG sensing. *SN Appl. Sci.* **2020**, *2* (3), 402.
(58) He, Q.; Zhang, Z.; Gao, F.; Li, Y.; Shi, J. In vivo biodistribution and urinary excretion of mesoporous silica nanoparticles: effects of particle size and PEGylation. *small* **2011**, *7* (2), 271−280.
(59) Kouchakzadeh, H.; Shojaosadati, S. A.; Maghsoudi, A.; Vasheghani Farahani, E. Optimization of PEGylation conditions for BSA nanoparticles using response surface methodology. *Aaps Pharmscitech* **2010**, *11*, 1206−1211.
(60) Bozuyuk, U.; Dogan, N. O.; Kizilel, S. Deep insight into PEGylation of bioadhesive chitosan nanoparticles: sensitivity study for the key parameters through artificial neural network model. *ACS Appl. Mater. Interfaces* **2018**, *10* (40), 33945−33955.
(61) Long, J.; Xiao, Y.; Liu, L.; Cao, Y. The adverse vascular effects of multi-walled carbon nanotubes (MWCNTs) to human vein endothelial cells (HUVECs) in vitro: role of length of MWCNTs. *J. Nanobiotechnol.* **2017**, *15* (1), 80.
(62) Ghaferi, M.; Raza, A.; Koohi, M.; Zahra, W.; Akbarzadeh, A.; Ebrahimi Shahmabadi, H.; Alavi, S. E. Impact of PEGylated liposomal doxorubicin and carboplatin combination on glioblastoma. *Pharmaceutics* **2022**, *14* (10), 2183.

https://doi.org/10.1021/acsomega.3c07432
ACS Omega 2024, 9, 1183−1195

(63) Kashkoulinejad-Kouhi, T.; Sawalha, S.; Safarian, S.; Arnaiz, B. A carbon-based nanocarrier for efficient gene delivery. *Therapeutic Delivery* **2021**, *12* (4), 311−323.
(64) Mirzaei, S.; Gholami, M. H.; Hashemi, F.; Zabolian, A.; Farahani, M. V.; Hushmandi, K.; Zarrabi, A.; Goldman, A.; Ashrafizadeh, M.; Orive, G. Advances in understanding the role of P-gp in doxorubicin resistance: Molecular pathways, therapeutic strategies, and prospects. *Drug Discovery Today* **2021**, *27* (2), 436−455.
(65) Zeng, X.; McCarthy, D. T.; Deletic, A.; Zhang, X. Silver/reduced graphene oxide hydrogel as novel bactericidal filter for point-of-use water disinfection. *Adv. Funct. Mater.* **2015**, *25* (27), 4344−4351.
(66) Debnath, S. K.; Srivastava, R. Drug delivery with carbon-based nanomaterials as versatile nanocarriers: progress and prospects. *Frontiers in Nanotechnology* **2021**, *3*, No. 644564.

https://doi.org/10.1021/acsomega.3c07432
ACS Omega 2024, 9, 1183−1195